

Which bright fast radio bursts repeat?

C.W. James,^{1*} S. Osłowski,^{2†} C. Flynn,² P. Kumar,² K. Bannister,³ S. Bhandari,³
 W. Farah,² M. Kerr,⁴ D.R. Lorimer,^{5,6} J.-P. Macquart,¹ C. Ng,⁷ C. Phillips,³
 D.C. Price,^{2,8} H. Qiu,^{3,9} R.M. Shannon² and R. Spiewak^{2,10}

¹International Centre for Radio Astronomy Research, Curtin University, Bentley, WA 6102, Australia

²Centre for Astrophysics and Supercomputing, Swinburne University of Technology, Mail H30, PO Box 218, VIC 3122, Australia

³CSIRO Astronomy & Space Science, Australia Telescope National Facility, P.O. Box 76, Epping, NSW 1710, Australia

⁴Space Science Division, Naval Research Laboratory, Washington, DC 20375, USA

⁵Department of Physics and Astronomy, West Virginia University, P.O. Box 6315, Morgantown, WV 26506, USA

⁶Center for Gravitational Waves and Cosmology, West Virginia University, Chestnut Ridge Research Building, Morgantown, WV 26505

⁷Dunlap Institute for Astronomy and Astrophysics, University of Toronto, 50 St. George Street, Toronto, ON M5S 3H4, Canada

⁸Department of Astronomy, University of California Berkeley, Berkeley CA 94720, USA

⁹Sydney Institute for Astronomy, School of Physics, University of Sydney, Sydney, NSW 2006, Australia

¹⁰ARC Centre of Excellence for Gravitational Wave Discovery (OzGrav)

Accepted XXX. Received YYY; in original form ZZZ

ABSTRACT

A handful of fast radio bursts (FRBs) are now known to repeat. However, the question remains — do they all? We report on an extensive observational campaign with the Australian Square Kilometre Array Pathfinder (ASKAP), Parkes, and Robert C. Byrd Green Bank Telescope, searching for repeat bursts from FRBs detected by the Comensal Real-time ASKAP Fast Transients survey. In 383.2 hr of follow-up observations covering 27 FRBs initially detected as single bursts, only two repeat bursts from a single FRB, FRB 171019, were detected, which have been previously reported by Kumar et al. We use simulations of repeating FRBs that allow for clustering in burst arrival times to calculate new estimates for the repetition rate of FRB 171019, finding only slight evidence for incompatibility with the properties of FRB 121102. Our lack of repeat bursts from the remaining FRBs set limits on the model of all bursts being attributable to repeating FRBs. Assuming a reasonable range of repetition behaviour, at most 60% (90% C.L.) of these FRBs having an intrinsic burst distribution similar to FRB 121102. This result is shown to be robust against different assumptions on the nature of repeating FRB behaviour, and indicates that if indeed all FRBs repeat, the majority must do so very rarely.

Key words: radio continuum: transients – methods: statistical

1 INTRODUCTION

Fast Radio Bursts (FRBs) are mysterious, bright bursts of radiation at radio wavelengths, discovered serendipitously just over a decade ago by Lorimer et al. (2007) at the Parkes telescope. FRBs have durations of a few hundred microseconds to tens of milliseconds, and dispersion measures (DMs) which can exceed the contribution due to the Interstellar Medium (ISM) of the Milky Way by more than an order of magnitude. Their high DMs are dominated by traversal of the pulse through the Intergalactic Medium (IGM) over cosmological distances (Shannon et al. 2018). At the time of

writing, there are nearly 100 FRBs listed in the FRB catalog at frbcat.org (Petroff et al. 2016). The progenitors of FRBs are currently unknown, with almost as many theories for their origins as there are observed FRBs (see Platts et al. (2018) and frbtheorycat.org for an extensive review).

To date, FRB observations from seven different facilities have been published. Chronologically, these are the Parkes radio telescope (Lorimer et al. 2007), the Robert C. Byrd Green Bank Telescope (GBT; Masui et al. 2015), the Arecibo Observatory (Spitler et al. 2014), the upgraded Molonglo synthesis telescope (UTMOST; Caleb et al. 2017), the Australian Square Kilometre Array Pathfinder (ASKAP; Bannister et al. 2017), the Canadian Hydrogen Intensity Mapping Experiment (CHIME; CHIME/FRB Collaboration et al. 2019a), and the Deep Synoptic Array ten-antenna

* E-mail: clancy.james@curtin.edu.au

† E-mail: stefanoslosowski@swin.edu.au

prototype (DSA-10; Ravi et al. 2019). FRBs have been seen at radio frequencies only, from 400 MHz to 8 GHz, despite extensive follow-up work at all other wavelengths (e.g. Bhandari et al. 2018).

No additional bursts were discovered at the location of any FRB until 9 repetitions from FRB 121102 were discovered at the 305-m Arecibo telescope (Spitler et al. 2016), in a source itself discovered earlier by Spitler et al. (2014). Since then, CHIME/FRB Collaboration et al. (2019a,b); Fonseca et al. (2020) have discovered 18 new repeating sources. The inferred all-sky rate of bursts observed by CHIME is too high to be consistent with models predicting once-off bursts (Ravi 2019). Most recently, in GBT follow-up observations, one of the ASKAP bursts, FRB 171019, has been observed to repeat (Kumar et al. 2019).

Despite these recent discoveries, FRB 121102, having been localised to its host galaxy at $z = 0.1927$ (Tendulkar et al. 2017; Chatterjee et al. 2017), remains by-far the best-studied FRB. The degree to which the properties of FRB 121102 relate to the other repeaters is currently unclear. At a more fundamental level, the question “which FRBs repeat?” remains unanswered, with an alternative hypothesis allowing for two or more populations.

Here, we test this hypothesis on the bright FRB population through deep follow-up observations for FRBs detected by The Commensal Real-time ASKAP Fast Transients (CRAFT) Survey. In Section 2, we describe the full set of observations from this follow-up program. Using a model for a repeating FRB developed in Section 3, we place limits on repetition rates — allowing for non-Poissonian burst-wait-time distributions — in Section 4.1. Importantly, by only analysing the probability of detecting multiple bursts from already identified FRBs, we eliminate the bias inherent in the initial detection. FRB 171019 is analysed similarly in Section 4.2, where we derive both lower and upper bounds on its repetition rate. We discuss our results in the wider context of models of repeating FRBs in Section 5.

2 CRAFT OBSERVATION PROGRAM

CRAFT is a very wide-area FRB survey using the Australian Square Kilometre Array Pathfinder (ASKAP) telescope (Macquart et al. 2010). At the time of writing, 28 FRBs have been reported (Bannister et al. 2017; Shannon et al. 2018; Macquart et al. 2019; Qiu et al. 2019; Bhandari et al. 2019; Agarwal et al. 2019; Bannister et al. 2019; Prochaska et al. 2019). The automated FRB search scheduling, and very wide search area on the sky, means that the locations of most detected FRBs have been observed extensively. This alone can be used to constrain the repetition rate (Bhandari et al. 2019; James 2019). No repeat bursts have been found for any previously reported FRBs in ASKAP data, which is inconsistent with all FRBs sources being similar to FRB 121102 (James 2019).

Compared to other FRB searches, ASKAP/CRAFT observations have a relatively high detection threshold — 26 Jy ms in Fly’s Eye mode (Shannon et al. 2018; James et al. 2019a), and no lower than 4.3 Jy ms in incoherent sum mode (Bannister et al. 2019). This is compensated for by having a high field of view (FOV), making it sensitive to the rarest, and (likely intrinsically) brightest, bursts. We have

therefore been pursuing an extensive follow-up program of CRAFT FRBs with Parkes and the GBT. These are both more sensitive telescopes, the limited FOVs of which are offset by CRAFT FRBs being localised to a few arcmin. They are also capable of observing a similar frequency range to that over which CRAFT FRBs have been discovered (0.8–1.4 GHz).

This CRAFT follow-up program has recently discovered two repeat bursts from one of the bright ASKAP/CRAFT FRBs, FRB 171019 (Kumar et al. 2019), with the CHIME collaboration also detecting a repeat burst (Patek & Chime/Frb Collaboration 2019). Additionally, one new burst, FRB 180318, has been discovered, which is unrelated to any of the previously observed bursts. The analysis of this FRB is ongoing, and will be reported elsewhere. However, no repeat bursts have been detected from any of the other CRAFT FRBs.

2.1 Follow-up observations

The data reported here cover ASKAP, Parkes, and GBT observations up to June 26th 2019, targeting the first 27 FRBs reported by the CRAFT collaboration up to and including FRB 180924. Observations at Parkes were recorded using the multibeam receiver (Staveley-Smith et al. 1996), which nearly overlaps with the CRAFT observations in terms of frequency coverage. The observations at GBT were performed mostly using the 800 MHz receiver, with a few observations performed at 1500 MHz. The Parkes observations were analysed in real-time using the standard transient pipeline based on HEIMDALL (Barsdell 2012) used by other surveys, most recently by Osłowski et al. (2019). GBT data were recorded for offline processing and searched for repeated bursts using the pipeline described in detail by Kumar et al. (2019). Table 1 summarises the relevant properties of the telescopes and Table 2 shows the total effective amount of time observed per source with the different follow-up facilities included in this analysis.

In a total of 383.2 hr of follow-up time (i.e. on instruments other than ASKAP), two repeat bursts, and one new FRB, were detected. The repeat bursts, both from FRB 171019, are reported elsewhere (Kumar et al. 2019), and the analysis of the new FRB is ongoing. Our key result, however, is that in this large follow-up campaign, and during ASKAP observations of the same field, only one FRB was detected to repeat. We thus proceed to derive limits on the repetition rates of each object, should they indeed repeat at all.

3 MODEL OF REPEATING FRBS

We base our model of a repeating FRB on the behaviour of FRB 121102. FRB 121102 resides in a dwarf galaxy host at a redshift of $z \approx 0.19$ (Chatterjee et al. 2017; Tendulkar et al. 2017). The bursts have DMs consistent with arising from a constant DM of 559.6 pc cm^{-3} , with an observational scatter of 4.2 pc cm^{-3} per burst (Hardy et al. 2017). The host galaxy has an apparent r band magnitude of $m_r = 25.1$ AB mag, and a stellar mass of $4.7 \times 10^7 M_\odot$ (Tendulkar et al. 2017). The H_α flux of the galaxy indicates a substantial contribution

Telescope	Receiver/ Mode	$\bar{\nu}$ [MHz]	$\Delta\nu$ [MHz]	δt [ms]	$\delta\nu$ [MHz]	F_{th} [Jy ms]
ASKAP	FE	1315	336	1.2565	1	21.9
	ICS	864–1320	336	0.864–1.728	1	$21.9N_{\text{ant}}^{-0.5}$
Parkes	MB	1382	337.1	0.064	0.39	0.5
GBT	820 MHz	820	200	0.08192	0.0977	0.12
	L-band	1500	800	0.08192	0.0977	0.058

Table 1. Observational properties of follow-up observations, for ASKAP Fly’s Eye (FE) and incoherent sum (ICS) modes (Shannon et al. 2018; Bannister et al. 2019); the Parkes multibeam (MB) receiver (Keane et al. 2017); and the Greenbank Telescope’s (GBT’s) 820 MHz primary focus and L-band receivers (Kumar et al. 2019). From left to right: the telescope and receiver names, the central frequency $\bar{\nu}$ and total bandwidth $\Delta\nu$, time- and frequency- resolutions δt and $\delta\nu$, and nominal sensitivity to a 1 ms duration burst.

FRB	ASKAP		Parkes	GBT	
	FE	ICS	MB	820	L
170107	883.5	7.3	30.0	10.9	4.3
170416	482.6	1.3	15.8	0.0	0.0
170428	912.9	1.5	12.2	3.5	1.3
170707	343.4	0.8	1.8	0.0	0.0
170712	205.7	2.1	4.6	0.0	0.0
170906	1148.4	3.6	4.1	3.0	1.3
171003	842.3	12.4	13.0	9.0	1.0
171004	949.0	12.6	16.6	9.8	1.0
171019	485.7	0.2	12.4	9.7	0.9
171020	1148.4	3.6	4.5	2.3	1.1
171116	1331.9	1.0	4.0	3.3	0.7
171213	965.3	0.0	4.0	3.8	0.3
171216	205.7	2.1	1.3	0.0	0.0
180110	1338.9	6.0	4.5	3.4	1.3
180119	965.3	0.0	3.9	5.7	0.3
180128.0	801.3	8.5	7.0	7.8	1.7
180128.2	343.4	0.8	2.8	0.0	0.0
180130	1338.9	6.0	3.4	3.7	1.3
180131	912.9	1.5	4.4	3.8	1.3
180212	783.4	6.8	7.9	7.4	1.2
180315	60.0	0.0	6.6	2.7	1.3
180324	49.0	1.4	3.6	7.0	1.0
180417	0.0	0.0	6.7	0.0	0.0
180430	10.9	0.0	1.0	8.3	1.4
180515	3.0	0.0	4.1	2.7	0.0
180525	737.8	9.8	4.8	5.1	2.0
180924	912.9	1.5	10.8	4.0	1.3
Total	18,162	90.6	238.7	118.4	26.1

Table 2. Total time of observations (hr) per telescope and target FRB. As some FRBs occurred in the same ASKAP field, some time spent observing with ASKAP covered multiple FRBs at once. See the caption of Table 1 for definitions of acronyms.

to the burst’s DM (due to the host) of up to 324 pc cm^{-3} (Tendulkar et al. 2017).

Since only one of the 27 ASKAP FRBs used in this analysis has been localised to its host galaxy, the model is written in terms of observable properties: fluence F , and rate in the observer frame R , at the mean frequency $\bar{\nu} = 1.296 \approx 1.3 \text{ GHz}$ at which most were discovered. We discuss the implications for the intrinsic properties of these sources in Section 5.1.

3.1 Fluence distribution

Given the range of telescope sensitivities used to observe CRAFT FRBs, and the variation in source distance expected from their DMs, the burst fluence distribution strongly affects the relative rates at which each telescope should detect repeat bursts. Law et al. (2017) presented a study of 17 repeated bursts from FRB 121102, estimating the cumulative slope of this distribution in log-log space to be $\gamma = -0.7$, with a burst rate above 10^{38} erg of approximately once per hour. We therefore describe the cumulative burst rate distribution R as

$$R(F_{1.3 \text{ GHz}}) = R_0 \left(\frac{F_{1.3 \text{ GHz}}}{1 \text{ Jy ms}} \right)^\gamma, \quad (1)$$

where $F_{1.3 \text{ GHz}}$ is the fluence at 1.3 GHz, R_0 is the rate of bursts with fluence above 1 Jy ms, and γ is the cumulative power-law index.

James et al. (2019b) have recently shown that s , being the ratio between the signal-to-noise ratio (S/N) of each burst, and the threshold S/N used in the detection algorithm, S/N_{th} , will follow the same power-law as the true underlying fluence distribution. This allows all data on FRB 121102 where these values have been published to be used to estimate γ . Applying this method to the nine VLA bursts from Law et al. (2017), and 21 bursts from Gajjar et al. (2018), James (2019) finds $\gamma = -0.91 \pm 0.17$.

Gourdji et al. (2019), using 29 bursts from a total sample of 41 bursts detected by Arecibo, estimate $\gamma = -1.8 \pm 0.3$. Using the s statistic, which allows the inclusion of all bursts while reducing potential sources of bias, produces $\gamma = -2.3_{-0.3}^{+0.4}$. This is clearly in conflict with previous results. It is also internally inconsistent with a power-law: the distribution of S/N within the sample is extremely peaked towards near-threshold events.

A population of FRBs repeating similarly to FRB 121102— i.e. as per equation (1) — will produce an intrinsic luminosity distribution for the FRB population with the same power-law index γ . Macquart & Ekers (2018) note that the FRB population must exhibit a burst strength index flatter than $\gamma = -1.5$ in order to obtain a cosmological distribution of bursts dominated by the intrinsically brightest events, as now found for the ASKAP/CRAFT sample by Shannon et al. (2018). Lu & Piro (2019) find $\gamma = -0.6 \pm 0.3$ for the intrinsic luminosity distribution of the ASKAP/CRAFT FRBs, and Lu & Kumar (2016) find $-1.2 \leq \gamma \leq -0.5$ for Parkes data.

In this work, we therefore consider the range $\gamma = -1 \pm 0.5$ to cover a broad range of possible burst strength indices, while noting the range $\gamma = -0.9 \pm 0.2$ is most likely.

3.2 Spectral properties

Bursts observed from FRB 121102 are contained in a relatively narrow frequency range (Law et al. 2017), and are typically composed of several temporal sub-bursts (Hessels et al. 2019). As all searches used in this work use the entire bandpass with equal weighting to evaluate burst S/N, spectral structure on frequency scales much smaller than the bandpass will not affect telescope sensitivity. However, the different observation frequencies and bandwidths require a model for how the burst rate scales between instruments.

To develop such a model, we use a power-law with spectral index α , such that the fluence at frequency ν is

$$F(\nu) = F_{1.3\text{GHz}} \left(\frac{\nu}{1.3\text{GHz}} \right)^\alpha. \quad (2)$$

We do not consider any low-frequency cut-off in the burst spectrum, as suggested by Sokolowski et al. (2018), since the CHIME collaboration have observed bursts down to 400 MHz (CHIME/FRB Collaboration et al. 2019a), below the frequency ranges of the observations reported here.

Macquart et al. (2019), analysing a sample of 23 ASKAP bursts almost identical to that used here, find $\alpha = -1.5^{+0.2}_{-0.3}$ from the distribution of spectral power within the 336 MHz wide ASKAP band. For FRB 171019, Kumar et al. (2019) find evidence for a much steeper spectral index than the nominal value of $\alpha = -1.5$, with most-likely values near $\alpha = -8$ or steeper. This cannot be typical of all ASKAP FRBs, nor typical of the population observed by CHIME down to 400 MHz, since far more bursts would then have been detected. It is also inconsistent with the non-detections of ASKAP FRBs by the Murchison Wide-field Array (Sokolowski et al. 2018). However, it is possible for a single, unusual object to have properties very different from that of the entire population. Therefore, we assume $\alpha = -1.5$ for the majority of FRBs in Section 4.1, and consider $0 \leq \alpha \leq -8$ for FRB 171019 in Section 4.2.

Equation (2) can be interpreted as either modelling the spectral index of individual broadband bursts, or as modelling the frequency-dependent rate of bursts individually contained within a narrow bandwidth through equation (1). The fluence thresholds F_{th} quoted in Table 1 are calculated assuming full band occupancy. Should observational bandwidth increase beyond the characteristic bandwidth of repeat bursts however, both the fluence threshold F_{th} , and number of bursts occurring within the bandwidth, will increase linearly. The former effect will act to decrease the observation rate, while the latter will increase it. For the fluence dependence given by equation (1), the total rate

$$R \propto \left(\frac{\Delta\nu}{336\text{MHz}} \right)^{\gamma+1}, \quad (3)$$

where the standard ASKAP bandwidth of 336 MHz is used as a normalisation constant. Given that γ is likely to be in the range -0.5 to -1.5 (see Section 3.2), the total rate will scale with bandwidth to the power of ± 0.5 .

For computational simplicity, we only consider two cases

in this work. The ‘standard’ case, using the nominal thresholds of Table 1 regardless of bandwidth, applies to broadband bursts, or to narrow-band bursts when $\gamma = -1$ through equation (3). We also consider a case where

$$F_{\text{th}} \propto \left(\frac{\Delta\nu}{336\text{MHz}} \right)^{0.5}, \quad (4)$$

which is equivalent to $\gamma = -2$. As noted in Section 3.1, this is disfavoured by current measurements, i.e. this scenario is perhaps overly pessimistic. This scenario is termed ‘low band occupancy’. It represents a burst occupying a small range of frequencies in the observation band, reducing the event rate with bandwidth when $\gamma = -2$. The ‘standard’ scenario also represents low band occupancy when $\gamma = 1$.

3.3 Arrival time distribution

The arrival-time distribution of bursts from FRB 121102 appears to be clustered, with bursts typically discovered in groups (e.g. Gajjar et al. 2018). Oppermann et al. (2018) find that a Weibull distribution describes the observed clustering of bursts, and measure a repeat rate of 6_{-2}^{+3} events per day for fluences > 20 mJy, and a clustering parameter k of $0.34^{+0.06}_{-0.05}$.

The Weibull distribution is commonly used in failure analysis. In this context, a value of $k < 1$ models cases where failure is likely to occur immediately (e.g. due to defects), with a failure rate decreasing over time, while $k > 1$ models cases where the failure probability increases with time, e.g. due to ageing. The case of $k = 1$ is a failure rate independent of time, i.e. a Poisson process. In the context of emission from a repeating FRB, $k < 1$ indicates a clustered distribution, with a high probability of short wait times between bursts, but also a high probability of long periods of inactivity, while $k = 1$ is the Poisson case with an exponential wait time distribution between bursts. Note that this is in contrast to a model with active and inactive periods, with the former having a higher emission rate than the latter, but with burst times being governed by a Poisson process within each period.

We model the potentially clustered nature of repeating FRBs using the same approach as Oppermann et al. (2018), i.e., the probability distribution P of wait times δt between successive bursts

$$P(\delta t | k, R) = \frac{k}{\delta t} \left[\delta t R \Gamma(1 + k^{-1}) \right]^k e^{-[\delta t R \Gamma(1 + k^{-1})]^k}, \quad (5)$$

where Γ is the gamma function. This parametrization holds R constant while changing k . For completeness, we investigate the range $k = 0.1$ – 1 .

3.4 Burst width and scattering

The sensitivity of an FRB search reduces with burst width, as a finite fluence is spread over more noise. The burst width is attributable to an intrinsic width, which we assume is frequency independent; scatter broadening, which will increase at lower frequencies as $\sim \nu^{-4.4}$; and dispersion smearing, due to the finite width of each frequency channel. The intrinsic durations of bursts (or groups of sub-bursts) from FRB 121102 are 1–5 ms (Hessels et al. 2019), with sub-burst

structure down to 0.1 ms. The bursts are not significantly affected by scattering.

The durations of bursts measured by ASKAP vary from approximately the 1.27 ms time resolution of the search to 5 ms, with a scattering tail detectable in the sample of Shannon et al. (2018) only for the brightest burst, FRB 180110. Here, we use the detected widths of ASKAP bursts to estimate telescope sensitivity at 1.3 GHz, and consider different sets of assumptions in scaling to other frequencies.

The three considered assumptions are that the burst widths observed by ASKAP contain no scattering contribution; that they are entirely scatter-dominated; and (the most pessimistic case) that they are scatter dominated at frequencies below 1.3 GHz, but limited by their intrinsic width at higher frequencies. In these scenarios, the observed frequency-dependent burst width $w_{\text{obs}}(\nu)$ is scaled from the ASKAP width w_{A} as

$$w_{\text{obs}}(\nu) = \begin{cases} w_{\text{A}} & \text{no scattering} \\ w_{\text{A}} \left(\frac{\nu}{1.3 \text{ GHz}} \right)^{-4.4} & \text{scattering} \\ w_{\text{A}} \text{ MAX} \left[1, \left(\frac{\nu}{1.3 \text{ GHz}} \right)^{-4.4} \right] & \text{pessimistic} \end{cases} \quad (6)$$

The width due to dispersion smearing within each frequency channel, w_{DM} , is given by

$$w_{\text{DM}} = 8.3 \mu\text{s} \frac{\text{DM}}{1 \text{ pc cm}^{-3}} \frac{\delta\nu}{1 \text{ MHz}} \left(\frac{\nu}{1 \text{ GHz}} \right)^{-3}, \quad (7)$$

where $\delta\nu$ is the channel width from Table 1.

3.5 Sensitivity dependence

For a given fluence, the sensitivity to a transient source scales with its effective duration w_{eff} as

$$F_{\text{th}} = F_{\text{th}}(1 \text{ ms}) \sqrt{\frac{w_{\text{eff}}}{1 \text{ ms}}}. \quad (8)$$

We model the total effective width of a burst, w_{eff} , following Cordes & McLaughlin (2003), using the geometric sum of its individual widths

$$w_{\text{eff}} = \sqrt{w_{\text{DM}}^2 + w_{\text{samp}}^2 + w_{\text{obs}}^2}, \quad (9)$$

where w_{DM} is the smearing of dispersion measure in each frequency channel (evaluated at band centre), w_{samp} is the time resolution used for the (incoherent) dedispersion search, and w_{obs} is given by equation (6).

3.6 Implementation in a simulation

Limits on the repetition properties are generated as follows. Each simulation run is characterised via the parameter set k , R , γ , a set of assumptions on band occupancy, burst width, and spectral index α , and the FRB in question.

The list of observations for that FRB for each telescope is loaded and sorted in chronological order. The nominal thresholds are then scaled to effective thresholds at 1.3 GHz using the observed width w and DM of each burst, and each observation's instrumental and detection parameters from Table 1. In the case of ASKAP ICS observations, the frequency, bandwidth, and number of telescopes N varied for each observation, and the effective threshold is calculated accordingly, using $F_{\text{th}} \sim N^{-0.5}$ (Bannister et al. 2019). The

F_{eff} Assumption	ASKAP		Parkes	GBT	
	FE	ICS	MB	820 MHz	L-band
Standard	64	13	0.82	0.28	0.11
Flat spectrum	64	13.5	0.75	0.56	0.87
No scattering	64	12.5	0.95	0.10	0.13
Pessimistic Scat.	64	13	0.95	0.28	0.13
Low band occupancy	64	13	0.83	0.28	0.17

Table 3. Effective telescope thresholds (Jy ms), to FRB 180128.0 (DM = 441.7 pc cm⁻³, $w_{\text{A}} = 2.9$ ms), i.e. telescope thresholds are scaled relative to ASKAP Fly's Eye observation parameters from Table 1, under different sets of assumptions. These are the 'standard' scenario ($\alpha = -1.5$, $w \propto \nu^{4.4}$, full band occupancy); setting a flat spectrum ($\alpha = 0$); no scattering ($w = w_{\text{A}}$), pessimistic scattering from equation (6); and low band occupancy from equation (3). The values for ASKAP ICS mode are typical examples. See Table 1 for definitions of acronyms.

sensitivity of each ASKAP observation is also scaled according to the sensitivity of the discovery beam, and position in that beam, according to James et al. (2019a). Due to an error in metadata, some observations with the Parkes multibeam were offset from the position of the FRB being followed-up. In these cases, the telescope threshold is increased to account for the reduced sensitivity away from beam centre. For most Parkes and all GBT observations however, the location of the FRB was sufficiently well-localised (see Shannon et al. 2018) that no beam correction is needed.

We use the central frequency only to characterise telescope sensitivity — for burst spectral indices in the range $-2 \leq \alpha \leq 0$, this leads to errors of less than 10% in assumed sensitivity for the GBT L-band receiver, and less than 1% for the other instruments. For the investigated range of γ , corresponding rate errors will be comparable. Since the GBT L-band receiver contributed only 7% of the total follow-up time, total expected rate errors will be at the 1% level.

An example of the effective thresholds F_{eff} calculated with this procedure are given in Table 3, for different sets of assumptions on burst width, band occupancy, and spectral index. By design, the sensitivity of ASKAP Fly's Eye observations is unaffected by this choice of assumption, since F_{eff} is normalised by these observing parameters. The variation in ASKAP ICS observations is due to some observations having lower frequency and/or a longer integration time. The Parkes multibeam, with similar bandwidth and observation frequency to ASKAP, also has an approximately constant F_{eff} . The telescope most affected is the GBT. Observations with the 800 MHz receiver are at a lower frequency, and L-band observations have a much broader bandwidth. This results in sensitivity varying by factors of 5–10 between different assumptions.

3.7 Simulation method

Beginning with the time of the FRB discovery, sequences of burst wait times are drawn according to equation (5), using the Weibull parameter k , and the rate R scaled from a nominal value above 1 Jy ms to the lowest value of effective telescope threshold. Time is defined relative to the initial discovery, and sequences must begin at that time. The Weibull distribution is statistically identical when generating bursts both forwards and backwards in time, and this is

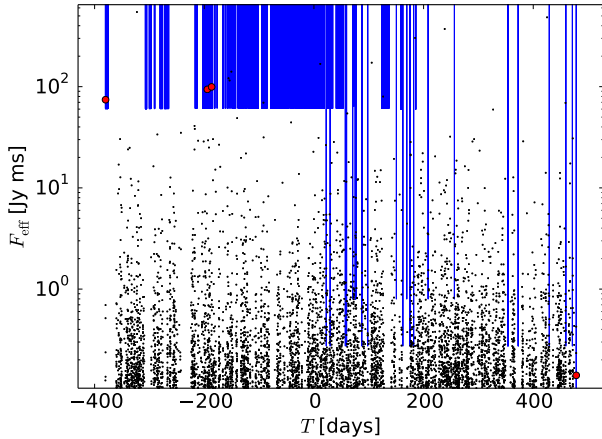


Figure 1. Illustration of the simulation of a sequence of bursts (black dots), compared to observations (blue lines), and detections (red circles). The observation lines have minima at the effective threshold, and span the time range observed. This case is for FRB 180119, for $R_0 = 1 \text{ day}^{-1}$, $k = 0.34$, $\gamma = -0.9$, and the standard set of assumptions. The original discovery, at time $T = 0$ days, is not shown. Note that many ASKAP observations are sufficiently close in time that the lines overlap.

done to cover all observations that would have been sensitive to that FRB, i.e. both before and after the initial discovery. The fluence of each burst generated during an observation period is sampled according to the differential power-law index of $\gamma - 1$. If that burst passes the telescope threshold, it is counted as a detection (the initial discovery is ignored). An example of such a sequence is shown in Fig. 1.

Discounting the initial discovery is a critical statistical step in our analysis. Since we do not estimate the population of repeating FRBs from which we observe no bursts at all, using the initial detections would create a bias towards high burst rates. Rather, these are used to identify the presence of a potentially repeating FRB, and we model the probability of a repeat burst given the time of the initial observation.

In order to obtain a good statistical estimate of the probability of detecting a repeat burst, 1000 such sequences are generated for each simulation run. The total number of sequences in which one or more repeat bursts are detected is recorded. The rate R is then increased until all 1000 such sequences produce more repeat bursts than observed for that FRB, and reduced until no repetitions are observed. These data are then used to fit probabilities $p(R|k, \gamma)$ of any given repetition outcome (e.g. no detected repeats) as a function of R for each k , γ , and set of assumptions. An example of these fits — performed with SciPy (Virtanen et al. 2019), with a 5th-order polynomial in $\log R - \log p/(1-p)$ space to obtain smooth results in both the limits $p \rightarrow 0$ and $p \rightarrow 1$ — is given in Fig. 2. The fits are reliable in the range $0.002 < p < 1$, allowing limits of up to 99.7% (3σ) confidence to be set.

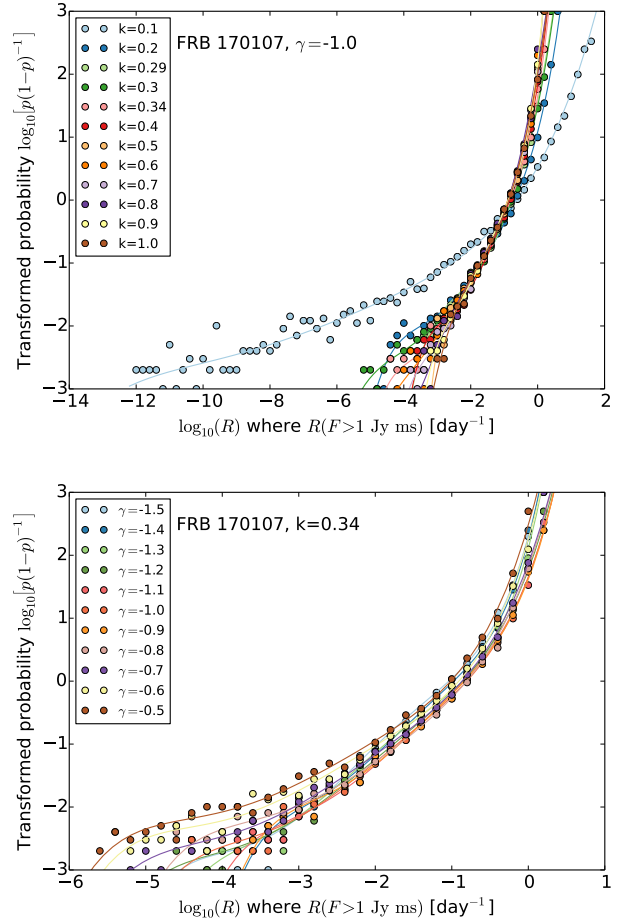


Figure 2. Probability $p(R|\gamma, k)$ of detecting one or more repeat bursts, as a function of burst rate R above 1 Jy ms, for FRB 170107. Top: varying k for fixed $\gamma = -0.9$; bottom: varying γ for fixed $k = 0.34$. Points are simulated probabilities, lines are fifth-order polynomial fits.

4 RESULTS

4.1 Limits on repetition for FRBs with no repeats

For those FRBs with no observed repeat bursts (all except FRB 171019), confidence limits on repetition rates R can be set when the probability of detecting one or more repeat bursts is equal to the desired level of confidence. Tests showed that quoting limits at the threshold of 1 Jy ms showed least variation with γ . Fig. 3 displays the 90% confidence upper limits, R_{90} , on the burst rate R above 1 Jy ms for FRB 170107. For the standard scenario ($\alpha = -1.5$, scattering as $\nu^{-4.4}$, full band occupancy, $k = 0.34$, $\gamma = -0.9$), R_{90} was found to be 0.56 day^{-1} . Holding k and γ constant and varying assumptions regarding scattering, band occupancy, and allowing spectral index to be 0, varied R_{90} between 0.43 day^{-1} and 0.60 day^{-1} , i.e. $^{+3}_{-25}\%$. This is comparable to the variation when allowing only k and γ to fluctuate within their nominal ranges of 0.29 to 0.4 and -0.7 to -1.1 respectively (R_{90} varying by $^{+13}_{-17}\%$). Allowing very clustered distributions ($k = 0.1$) results in weaker limits for $\gamma < -0.9$, with $R_{90} = 6 \text{ day}^{-1}$ for $\gamma = -1.5$. This is because more-negative

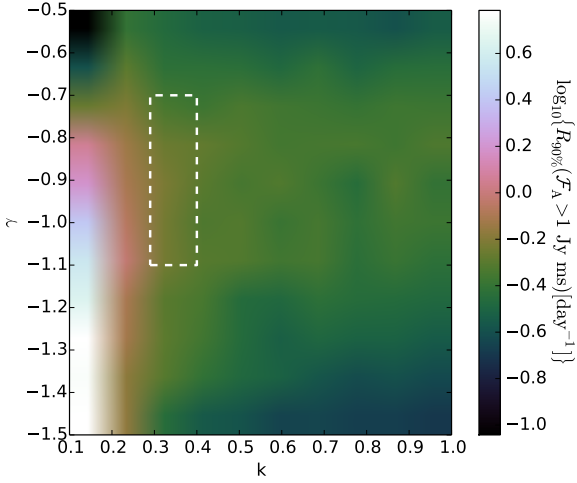


Figure 3. Upper limits at 90% confidence, R_{90} , on the repetition rate R of bursts above 1 Jy ms from FRB 170107 as a function of k and γ . The white dashed box indicates the ranges on these parameters for FRB 121102 — see Section 3.

values of γ place emphasis on the more sporadic follow-up observations with Parkes and GBT, which could easily miss an outburst. The strongest limits of $R_{90} = 0.09 \text{ day}^{-1}$ are placed for $\gamma = -0.5$, $k = 0.1$, since no secondary bursts were detected by ASKAP close to the initial detection.

Given the dominance of uncertainties in k and γ , for other FRBs in the sample, we only simulate the ‘standard’ scenario. Table 4 reports 90% confidence upper limits, R_{90} , on the repetition rate above 1 Jy ms, and the variation in R_{90} when varying (k, γ) over the ranges (0.29 to 0.34, -1.1 to -0.7), and (0.1 to 1, -1.5 to -0.5), respectively. The differences in limits between FRBs reflect the integration times from Table 2 and telescope sensitivities from Table 1.

4.2 Limits on repetition for FRB 171019

In the case of FRB 171019, limits on burst properties can be derived considering that precisely two repeat bursts were observed; that these bursts were observed by the GBT 800 MHz receiver; and that the bursts were observed on 2018-07-20 at 08:33:37 UT (observation of 1200 s duration) and 2019-06-09 at 07:40:46 UT (observation of 8397 s duration). The first piece of information allows both upper and lower rate limits to be set for any given k , γ , and α . It also disfavors small values of k distributions, since such clustered distributions tend to produce either no or many repeats.

The second clearly constrains the valid range of γ and α , and will favour steep spectral indices for both, since the bursts were observed in the lowest-frequency observation only, and the far more numerous ASKAP Fly’s Eye observations made at only slightly higher frequencies were at a lower sensitivity.

The third also disfavors clustered burst arrival times, since these would likely be observed in the same observation period.

We simulate burst sequences for FRB 171019 as per Section 3.7 as a grid in k - γ - α , recording the fraction of bursts satisfying the above criteria. Since it is computationally in-

k	0.34	$0.29 \leq k \leq 0.4$		$0.1 \leq k \leq 1$	
γ	-0.9	$-0.7 \leq \gamma \leq -1.1$		$-0.5 \leq \gamma \leq -1.5$	
FRB	R_{90}	R_{90}^{\min}	R_{90}^{\max}	R_{90}^{\min}	R_{90}^{\max}
170107	0.56	0.5	0.63	0.091	6.1
170416	3.1	2.4	5.3	0.095	67
170428	1.3	0.95	1.8	0.38	16
170707	8.4	5.3	16	1.5	140
170712	6.3	5.4	12	2.0	130
170906	1.2	0.97	1.7	0.03	10
171003	0.96	0.82	1.2	0.046	9.4
171004	0.66	0.6	0.83	0.026	4.0
171020	2.4	2.1	2.8	0.15	37
171116	1.5	1.0	2.4	0.023	14
171213	1.8	1.4	2.1	0.056	20
171216	13	8.3	31	0.14	200
180110	1.9	1.4	2.8	0.038	23
180119	1.2	0.92	1.7	0.026	10
180128.0	1.2	0.97	1.4	0.046	11
180128.2	6.4	4.5	15	0.029	78
180130	1.7	1.2	2.4	0.029	18
180131	1.9	1.6	2.9	0.042	24
180212	1.2	1.0	1.4	0.089	10
180315	2.9	2.5	3.8	0.55	47
180324	3.1	2.4	3.7	0.85	57
180417	18	14	23	4.7	2400
180430	1.7	1.1	2.6	0.3	47
180515	6.9	5.8	9.7	1.2	190
180525	2.6	2.3	3.9	0.62	49
180924	2.0	1.6	3.1	0.46	110

Table 4. Upper limits at 90% confidence, R_{90} , on the repetition rate R above 1 Jy ms for each FRB for different ranges of Weibull index k and burst fluence index γ , assuming the standard parameter set with $\nu^{-4.4}$ scattering, spectral index $\alpha = -1.5$, and full band occupancy. These have estimated systematic uncertainties of $\pm 25\%$ due to different assumptions regarding band occupancy, burst width, and spectral index α .

tensive to recreate the exact observation times of repeat bursts, we count all instances where two bursts are detected by the GBT at 800 MHz in two different observations as satisfying our constraints. We again fit the simulated probability as a function of R , $P(R|k, \gamma, \alpha)$, and use its maximum, $P_{\max}(k, \gamma, \alpha)$, to set confidence limits.

Fig. 4 shows $P_{\max}(k, \gamma, \alpha)$ for three values of k . The global probability is maximised at 24.7% for $\alpha = -6.5$, $k = 1$ (Poisson), $\gamma = -1.4$, and $R(F > 1 \text{ Jy ms}) = 4.27 \cdot 10^{-2}$, although there is a broad maximum for small values of γ , α , and large values of k . Both the steep spectrum and the Poissonian burst time distribution is consistent with the analysis of Kumar et al. (2019).

At the nominal value of $k = 0.34$, the probabilities vary little in α - γ space, with only large values of γ strongly disfavoured.

Interestingly, for $k \leq 0.2$, less-negative values of α become favoured. This is because it becomes more plausible to have a higher expected detection rate for the > 1 GHz Parkes and GBT observations, which just happen to miss periods of outburst, and a lower expectation for GBT 800 MHz observations, which luckily happens to barely catch two outbursts. Since ASKAP observations were widely spread in time, it becomes difficult to avoid these with unlucky outburst timing, so that $\gamma = -1.5$ becomes strongly favoured.

The estimated probabilities p correspond to the likeli-

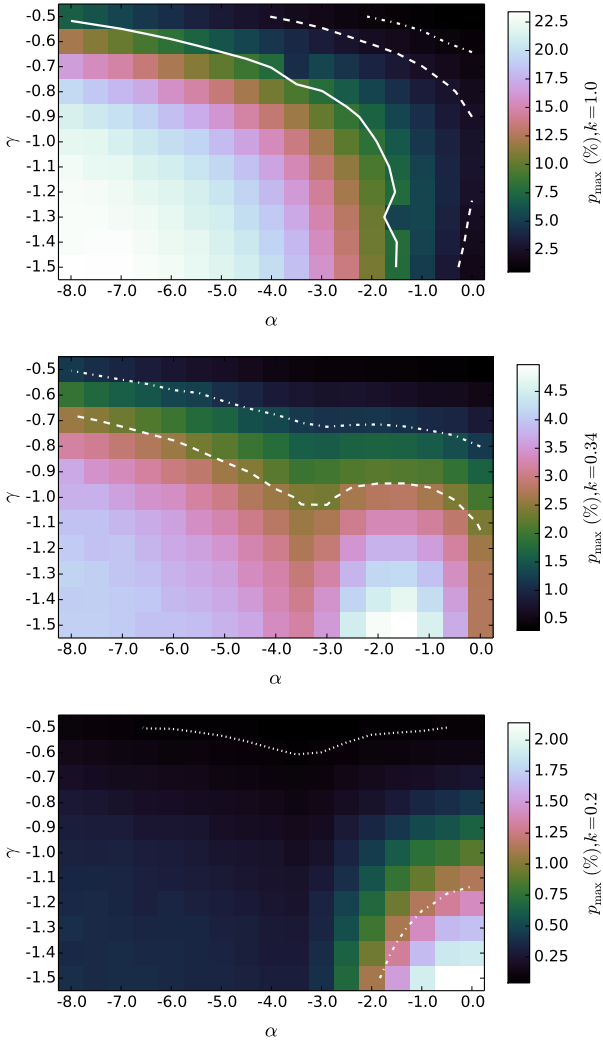


Figure 4. Simulated probability of CRAFT follow-up observations of FRB 171019 after marginalisation over R , $p_{\max}(\alpha, \gamma)$, for three values of Weibull burst index: $k = 1$ (top), $k = 0.34$ (middle), and $k = 0.2$ (bottom). The solid, dashed, dot-dash, and dotted contours respectively indicate 68%, 90%, 95%, and 99.7% exclusion regions.

hood of an observation given a particular hypothesis on R , α , γ , and k . Confidence intervals can therefore be calculated using Wilks’ theorem (Wilks 1962), which states that in the large-sample limit, the test statistic

$$\Delta D \equiv 2 [\log p(R, \alpha, \gamma, k)_{\max} - \log p(\alpha, R, \gamma, k)_{\text{true}}] \sim \chi_4^2, \quad (10)$$

where the subscript ‘max’ indicates the parameter values maximising the probability p , and ‘true’ indicates the true value of these parameters. The R - α - γ - k space sets the degrees of freedom for the χ^2 distribution to four. This is used to generate the confidence regions in Fig. 4. In Appendix A, we show that this procedure results in slightly conservative limits.

Marginalising over all other parameters, the allowed ranges at 68% confidence are $k > 0.4$, $\alpha < -1$, with no constraints on γ ($\gamma = -0.5$ is barely allowed for $\alpha = -8.0$, $k = 1$). At 90% C.L., only $k = 0.1$ can be excluded.

FRB	z_{\max}	$R_{90}(E > 10^{39} \text{ erg}) [\text{day}^{-1}]$		
		$\gamma = -0.7$	$\gamma = -0.9$	$\gamma = -1.1$
170107	0.517	1.5	2.3	2.8
170416	0.441	4.3	8.8	14
170428	0.855	7.1	18	39
170707	0.179	1.7	3.3	4.7
170712	0.251	4.2	5.1	7.2
170906	0.322	0.956	1.7	2.4
171003	0.387	1.5	2.0	2.4
171004	0.243	0.42	0.499	0.515
171019 [†]	0.385	$1^{+1.3}_{-0.7}$	$1.4^{+1.7}_{-0.9}$	$1.5^{+2.0}_{-0.9}$
171020	0.0636	0.181	0.12	0.0571
171116	0.525	2.4	6.2	11
171213	0.107	0.248	0.245	0.154
171216	0.149	1.9	3.5	5.2
180110	0.611	4.7	12	19
180119	0.333	1.0	1.8	2.6
180128.0	0.368	1.5	2.2	2.5
180128.2	0.417	6.5	16	36
180130	0.279	0.824	1.7	2.0
180131	0.56	4.2	9.6	17
180212	0.115	0.228	0.188	0.117
180315	0.401	6.5	6.7	6.3
180324	0.358	5.3	5.4	4.5
180417	0.398	33	40	36
180430	0.206	1.5	0.906	0.49
180515	0.29	7.9	7.6	6.2
180525	0.32	3.9	3.6	3.4
180924*	0.3214	3.2	2.8	2.2

Table 5. Estimated maximum redshifts, z_{\max} , of each FRB, and corresponding 90% C.L. upper limits on the intrinsic FRB rate R_0 (also given in Fig. 5) as a function of γ , for $k = 0.34$ and other standard parameters. [†]Best-fit repetition rate, and 90% confidence limits. *As it has been localised, the true redshift of FRB 180924 is used.

The nominal parameter set of $k = 0.34$, $\gamma = -0.9$, $\alpha = -1.5$ lies on the 90% exclusion level. The rate maximising this probability is $R(F > 1 \text{ Jy ms}) = 0.9 \text{ day}^{-1}$, significantly less than that of FRB 121102.

5 DISCUSSION

5.1 Absolute rates

A distance estimate to each FRB is required in order to translate our limits on rates above a given fluence observed at Earth into limits on the intrinsic rate above some energy. However, only one FRB in the sample, FRB 180924, has a confidently identified host (at $z = 0.3214$; Bannister et al. 2019). Nonetheless, a maximum distance to each can be estimated by attributing all non-Milky Way DM contributions to the intergalactic medium (IGM). Using the NE2001 model of Cordes & Lazio (2002), attributing a halo contribution equal to the minimum of 50 pc cm^{-3} (Prochaska & Zheng 2019), and ignoring any host galaxy contribution, allows the DM- z relation due to the IGM from Inoue (2004) to be used to estimate a maximum redshift, z_{\max} . These are given in Table 5. Note that limits on the intrinsic FRB behaviour become weaker as the assumed distance to the source increases, so that using $z = z_{\max}$ leads to upper limits on the intrinsic rate.

The observational limits in Table 4 are rates above

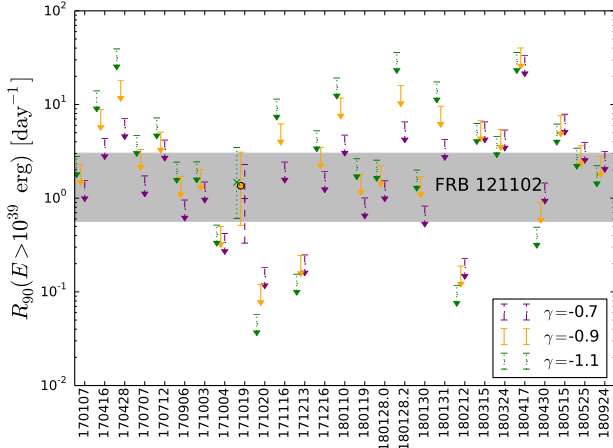


Figure 5. Points: upper limits at 90% confidence on the intrinsic rate R above an energy threshold of $E = 10^{38}$ erg, for three different values of γ . This is compared to the range of values estimates for FRB 121102 (grey shaded region — see Section 3).

1 Jy ms, which translates to an energy threshold E given by the fluence-energy relation of Macquart & Ekers (2018),

$$E = 4\pi D_L^2 F \frac{\Delta\nu}{(1+z)^{2+\alpha}}, \quad (11)$$

for luminosity distance D_L , assumed bandwidth $\Delta\nu = 336$ MHz, and a burst occupying the entirety of $\Delta\nu$ with spectral dependence α . The intrinsic rate R is also increased by $1+z$ to account for time dilation. The final limits are scaled to a rate above $E = 10^{39}$ erg using $\gamma = -0.9 \pm 0.2$. The results are shown in Fig. 5.

For FRBs with high DM/z_{\max} , the limiting fluence of 1 Jy ms translates to energies $> 10^{39}$ erg, so that limiting rates scaled to this threshold then get weaker as γ decreases. The converse is true for low-DM FRBs. The largest effect of γ is therefore a factor of 5.5 difference in R_{90} for the highest-DM FRB in the sample, 170428, with a DM of 991.7 pc cm^{-3} . This effect dominates over variation in limits due to $0.29 \leq k \leq 0.4$. For very bursty distributions ($k = 0.1$), the limits become significantly stronger when observations are clustered about the initial detection, and weaker when they are not. However, such behaviour is at odds with the behaviour of the three best-studied repeaters, FRB 121102 (Oppermann et al. 2018), FRB 180814.J0422+73 (CHIME/FRB Collaboration et al. 2019b), and FRB 180916.J0158+65 (The CHIME/FRB Collaboration et al. 2020), so from hereon we quote only limits for $k = 0.34$, equivalent to $0.29 \leq k \leq 0.4$.

The range of rates measured for FRB 121102 is shown as a grey band spanning $4.5\text{--}24 \text{ day}^{-1}$ above 10^{38} erg, covering estimates from Law et al. (2017), Gajjar et al. (2018), Oppermann et al. (2018), and James (2019), scaled to rates above 10^{39} erg using $\gamma = -0.9$. A total of 4 FRBs in our sample can be excluded at 90% confidence as being repeating FRBs with repetition rates similar to that of FRB 121102. For a further seven, part of the rate range of FRB 121102 can be excluded.

For FRB 171019, its maximum redshift, $z_{\max} = 0.385$, is much greater than that of FRB 121102, with $z = 0.193$

(Tendulkar et al. 2017). Hence, despite its observed rate being lower, its intrinsic rate may be identical to that of FRB 121102. It may, however, be much closer, and hence have a significantly lower intrinsic rate.

5.2 Do all Fast Radio Bursts repeat?

Other works have examined the question of whether or not all FRBs repeat similarly to FRB 121102. Palaniswamy et al. (2018) consider individual bursts detected by Parkes, and compare the limits these once-off bursts set on the wait time between bursts Δt , and the flux ratio between successive bursts S_i/S_{i+1} , with the measured values for FRB 121102. The authors cite an absence of singly observed bursts in the space $S_i/S_{i+1} < 1$, $\Delta t \lesssim 10^4$ s as evidence for distinct populations. However, for a singly observed burst, the non-detection of a second ($i+1$) burst necessarily limits its flux S_{i+1} to be less than that of the observed burst, S_i , by definition. However, the non-observation of any preceding burst also requires a point at $S_{i-1}/S_i < 1$. The omission of points corresponding to preceding bursts creates a bias, resulting in an apparent, but illusory, disparity between singly observed bursts and those from FRB 121102. Furthermore, Palaniswamy et al. (2018) do not account for the greater distance at which the Parkes sample of FRBs is detected (Shannon et al. 2018). Objects intrinsically identical to FRB 121102, but located at a greater distance, will exhibit a lower apparent rate, thus accounting for the absence of bursts in the interval $\Delta t \lesssim 10^4$ s. By not accounting for distance effects, their result leaves open the possibility that Parkes FRBs come from objects intrinsically identical to FRB 121102, but which are generally more distant.

This is the conclusion of Lu & Kumar (2016), who use a cosmological FRB source evolution proportional to the core-collapse supernova rate, and find that Parkes data are consistent with all repeaters being intrinsically similar to FRB 121102 at the 5–30% level.

Our observations here exclude this possibility, since four FRBs in the CRAFT survey cannot repeat with the regularity of FRB 121102.

This does not necessarily mean that they do not repeat at all. Models of FRBs powered by young neutron stars (Cordes & Wasserman 2016; Connor et al. 2016; Pen & Connor 2015) or magnetar flares (Popov & Postnov 2010; Thornton et al. 2013; Kulkarni et al. 2014; Metzger et al. 2017) would be expected to produce fewer, weaker bursts as they age through spin-down or magnetic field decay. This should then produce a population Φ of repeating FRBs with a distribution of repetition rates, similarly to the observed population of pulsars and magnetars. Indeed, in their specific model, Lu & Kumar (2016) find some evidence that the mean repetition rate of FRBs must be less than FRB 121102.

James (2019) argues that a rate distribution according to $\Phi(R) \sim R^{-2} dR$ is consistent with the number of single bursts observed in the CRAFT lat50 survey of Shannon et al. (2018). Note this is not the distribution of rate as a function of energy for a given FRB, but the distribution of rates above a fixed energy over the population of FRBs.

In this model, FRB 121102 would be a rare, rapidly repeating object, as may be FRB 180814.J0422+73 (CHIME/FRB Collaboration et al. 2019b) and FRB 180916.J0158+65 (The CHIME/FRB Collabora-

tion et al. 2019), while the remaining seven repeating CHIME FRBs may be more numerous, less-frequently repeating objects. Whether or not the model is quantitatively consistent with the observed number of both once-off and repeating CHIME FRBs would require more-detailed estimates of the CHIME survey’s sensitivity, sky coverage, and effective observing time than are currently present in the literature.

Is this model consistent with the follow-up observations presented here? While the volumetric number density of repeating objects scales as $R^{-2}dR$, the number of bursts produced by each FRB scales with R by definition. Hence, the probability that a burst comes from an FRB with intrinsic rate R scales as $R^{-1}dR$. That is, each observed single burst has equal probability of being attributable to a given range in $d \log R$. To detect one repeating FRB, and exclude four, from having a repetition rate similar to that of FRB 121102, suggests that at most 60% of all repeating FRBs would be expected to have this rate (90% C.L.). Hence, the rate distribution for repeating FRBs must extend over at least two orders of magnitude in repetition rate, given the expected flatness in $\log(R)$. In other words, while all FRBs may indeed repeat — it is, after all, observationally impossible to exclude an arbitrarily low repetition rate — a sizeable fraction of FRBs must repeat with a low rate, or else come from a separate population of once-off progenitor events.

5.3 Model dependence

Our limits on the repetition rate R have been calculated over a broad parameter space in burst spectrum (α), energy dependence of the burst rate (γ), and time-clustering (k). Nonetheless, there is no guarantee that the true behaviour of repeating FRBs lies within this space. How robust are our results to deviations from our model?

Firstly, regardless of the validity of the Weibull distribution as a quantitative model for burst wait times, these observations show evidence against clustering. The primary evidence is viewing many one-off bursts, where clustering of any form would tend to favour either viewing many bursts, or none at all. The detection of repeat bursts from FRB 171019 over a broad spread of observation times also lends credence to this.

Of particular note is that [The CHIME/FRB Collaboration et al. \(2020\)](#) have recently detected periodic emission from FRB 180916.J0158+65. Should an FRB observed by ASKAP behave similarly, it must necessarily have been observed in an active state. While we have not set limits as a function of potential periodicity between active and inactive states, any such limits on the time-averaged rate will be stronger than those presented here.

Secondly, these observations cover a relatively small spectral range, between 720 and 1900 MHz, and we emphasise that all rates are quoted relative to ASKAP observation parameters at 1.3 GHz. This both makes our conclusions more robust to spectral dependencies in FRB behaviour, but also completely insensitive to effects outside this range. In particular, the power-law spectral model does not appear to extend down to 184 MHz ([Sokolowski et al. 2018](#)). Furthermore, for spectral models where most bursts are expected below 1 GHz, the limited time-coverage of GBT 820 MHz observations will make limits more sensitive to the time struc-

ture of bursts. This is not the case for bursts above 1 GHz, where observations have a more uniform time-coverage.

Thirdly, while the energy dependence of the burst rate is consistent between FRB 121102 and the entire FRB population, it is clearly possible for a single FRB to exhibit properties that deviate significantly from the population mean. An example is the unusually steep spectral index for FRB 171019 considered here. Similarly, any given FRB could incur an excess DM and hence be located at a significantly lower redshift than is assumed when calculating absolute limits on the rate. Therefore, it is feasible that a small number of FRBs could violate the upper limits derived here. However, as a whole sample, the derived limits are relatively robust.

6 CONCLUSIONS

We have used the results of a survey of 27 ASKAP FRBs with the Robert C. Byrd Green Bank Telescope (GBT) and Parkes telescope to investigate FRB repetition. Only one FRB, 171019, has been detected to repeat, the details of which have already been reported by [Kumar et al. \(2019\)](#). We have used a simulation of repeating FRBs, combined with exact observation parameters, to set limits on the repetition properties of these 27 objects. In particular, we allow for clustered distributions of burst arrival times.

For four of the 26 FRBs not observed to repeat, we can exclude repetition rates comparable to that of FRB 121102, i.e. $R(E > 10^{39} \text{ erg}) < 0.5 \text{ day}^{-1}$. This assumes burst fluence indices $-1.1 \leq \gamma \leq -0.7$ and arrival time clustering $0.29 \leq k \leq 0.4$, consistent with observations of known FRBs. For FRB 171019, the parameters of FRB 121102 estimated by [Law et al. \(2017\)](#) and [Oppermann et al. \(2018\)](#) are only consistent with observations at the $\sim 10\%$ level. Clustering of burst arrival times are disfavoured, but cannot be excluded.

Our results — even including the one detected repeating object — set strong limits on the model of all bursts being attributable to repeating FRBs, with at most 60% (90% C.L.) of these FRBs having an intrinsic burst distribution similar to FRB 121102. We cannot exclude however that individual FRBs may repeat at much higher rates in parts of the spectrum unprobed by these observations, e.g. $< 700 \text{ MHz}$, or $> 2 \text{ GHz}$, or do so with burst energy distributions more complex than the power laws investigated here.

ACKNOWLEDGEMENTS

The Parkes radio telescope is part of the Australia Telescope National Facility which is funded by the Australian Government for operation as a National Facility managed by CSIRO. Part of this work was performed on the OzSTAR national facility at Swinburne University of Technology. OzSTAR is funded by Swinburne University of Technology and the National Collaborative Research Infrastructure Strategy (NCRIS). The Australian SKA Pathfinder is part of the Australia Telescope National Facility which is managed by CSIRO. Operation of ASKAP is funded by the Australian Government with support from the National Collaborative Research Infrastructure Strategy. ASKAP uses the resources

of the Pawsey Supercomputing Centre. Establishment of ASKAP, the Murchison Radio-astronomy Observatory and the Pawsey Supercomputing Centre are initiatives of the Australian Government, with support from the Government of Western Australia and the Science and Industry Endowment Fund. We acknowledge the Wajarri Yamatji people as the traditional owners of the Observatory site. The Green Bank Observatory is a facility of the National Science Foundation operated under cooperative agreement by Associated Universities, Inc. Work at NRL is supported by NASA. R.S. acknowledges support through ARC grants FL150100148 and CE170100004. This research has made use of NASA's Astrophysics Data System Bibliographic Services. This research made use of Python libraries MATPLOTLIB (Hunter 2007), NUMPY (van der Walt et al. 2011), and SCIPY (Virtanen et al. 2019).

REFERENCES

- Agarwal D., et al., 2019, *MNRAS*, p. 2216
- Bannister K. W., et al., 2017, *ApJ*, 841, L12
- Bannister K. W., et al., 2019, *Science*, 365, 565
- Barsdell B. R., 2012, PhD thesis, Swinburne University of Technology
- Bhandari S., et al., 2018, *MNRAS*, 475, 1427
- Bhandari S., Bannister K. W., James C. W., Shannon R. M., Flynn C. M., Caleb M., Bunton J. D., 2019, *MNRAS*, 486, 70
- CHIME/FRB Collaboration et al., 2019a, *Nature*, 566, 230
- CHIME/FRB Collaboration et al., 2019b, *Nature*, 566, 235
- Caleb M., et al., 2017, preprint, ([arXiv:1703.10173](https://arxiv.org/abs/1703.10173))
- Chatterjee S., et al., 2017, *Nature*, 541, 58
- Connor L., Sievers J., Pen U.-L., 2016, *MNRAS*, 458, L19
- Cordes J. M., Lazio T. J. W., 2002, ArXiv Astrophysics e-prints,
- Cordes J. M., McLaughlin M. A., 2003, *ApJ*, 596, 1142
- Cordes J., Wasserman I., 2016, Monthly Notices of the Royal Astronomical Society, 457, 232
- Fonseca E., et al., 2020, *ApJ*, 891, L6
- Gajjar V., et al., 2018, *ApJ*, 863, 2
- Goudji K., Michilli D., Spitler L. G., Hessels J. W. T., Seymour A., Cordes J. M., Chatterjee S., 2019, *ApJ*, 877, L19
- Hardy L. K., et al., 2017, *MNRAS*, 472, 2800
- Hessels J. W. T., et al., 2019, *ApJ*, 876, L23
- Hunter J. D., 2007, *Computing in Science and Engineering*, 9, 90
- Inoue S., 2004, *MNRAS*, 348, 999
- James C. W., 2019, *MNRAS*, 486, 5934
- James C. W., et al., 2019a, *Publ. Astron. Soc. Australia*, 36, e009
- James C. W., Ekers R. D., Macquart J.-P., Bannister K. W., Shannon R. M., 2019b, *MNRAS*, 483, 1342
- Keane E. F., et al., 2017, preprint, ([arXiv:1706.04459](https://arxiv.org/abs/1706.04459))
- Kulkarni S. R., Ofek E. O., Neill J. D., Zheng Z., Juric M., 2014, preprint, ([arXiv:1402.4766](https://arxiv.org/abs/1402.4766))
- Kumar P., et al., 2019, arXiv e-prints, p. [arXiv:1908.10026](https://arxiv.org/abs/1908.10026)
- Law C. J., et al., 2017, *ApJ*, 850, 76
- Lorimer D. R., Bailes M., McLaughlin M. A., Narkevic D. J., Crawford F., 2007, *Science*, 318, 777
- Lu W., Kumar P., 2016, *MNRAS*, 461, L122
- Lu W., Piro A. L., 2019, *ApJ*, 883, 40
- Macquart J.-P., Ekers R., 2018, *MNRAS*, 480, 4211
- Macquart J.-P., et al., 2010, *Publ. Astron. Soc. Australia*, 27, 272
- Macquart J.-P., Shannon R. M., Bannister K. W., James C. W., Ekers R. D., Bunton J. D., 2019, *ApJ*, 872, L19
- Masui K., et al., 2015, preprint, ([arXiv:1512.00529](https://arxiv.org/abs/1512.00529))
- Metzger B. D., Berger E., Margalit B., 2017, *ApJ*, 841, 14
- Oppermann N., Yu H.-R., Pen U.-L., 2018, *MNRAS*, 475, 5109
- Osłowski S., et al., 2019, *MNRAS*, 488, 868
- Palaniswamy D., Li Y., Zhang B., 2018, *ApJ*, 854, L12
- Patek C., Chime/Frb Collaboration 2019, The Astronomer's Telegram, 13013, 1
- Pen U.-L., Connor L., 2015, *ApJ*, 807, 179
- Petroff E., et al., 2016, *Publ. Astron. Soc. Australia*, 33, e045
- Platts E., Weltman A., Walters A., Tendulkar S. P., Gordin J. E. B., Kandhai S., 2018, preprint, ([arXiv:1810.05836](https://arxiv.org/abs/1810.05836))
- Popov S. B., Postnov K. A., 2010, in Harutyunian H. A., Micaelian A. M., Terzian Y., eds, Evolution of Cosmic Objects through their Physical Activity. pp 129–132 ([arXiv:0710.2006](https://arxiv.org/abs/0710.2006))
- Prochaska J. X., Zheng Y., 2019, *MNRAS*, 485, 648
- Prochaska J. X., et al., 2019, *Science*, 365, aay0073
- Qiu H., Bannister K. W., Shannon R. M., Murphy T., Bhandari S., Agarwal D., Lorimer D. R., Bunton J. D., 2019, *MNRAS*, 486, 166
- Ravi V., 2019, *Nature Astronomy*, p. 405
- Ravi V., et al., 2019, *Nature*, 572, 352
- Shannon R. M., et al., 2018, *Nature*, 562, 386
- Sokolowski M., et al., 2018, *ApJ*, 867, L12
- Spitler L. G., et al., 2014, *ApJ*, 790, 101
- Spitler L. G., et al., 2016, *Nature*, 531, 202
- Staveley-Smith L., et al., 1996, *Publ. Astron. Soc. Australia*, 13, 243
- Tendulkar S. P., et al., 2017, *ApJ*, 834, L7
- The CHIME/FRB Collaboration et al., 2019, arXiv e-prints, p. [arXiv:1908.03507](https://arxiv.org/abs/1908.03507)
- The CHIME/FRB Collaboration et al., 2020, arXiv e-prints, p. [arXiv:2001.10275](https://arxiv.org/abs/2001.10275)
- Thornton D., et al., 2013, *Science*, 341, 53
- Virtanen P., et al., 2019, arXiv e-prints, p. [arXiv:1907.10121](https://arxiv.org/abs/1907.10121)
- Wilks S., 1962, *Mathematical Statistics*. John Wiley and Sons Ltd
- van der Walt S., Colbert S. C., Varoquaux G., 2011, *Computing in Science and Engineering*, 13, 22

APPENDIX A: DISTRIBUTION OF THE TEST-STATISTIC D

In this work, we use Wilks' theorem (Wilks 1962) to assume a χ^2 distribution for the test-statistic D given in equation (10). For the analysis of Section 4.2, a likelihood maximisation is performed over the parameter set R , α , γ , and k , such that $D \sim \chi_4^2$. Wilks' theorem states that D will reach this asymptotic form only as the number of data points used in the maximisation tends to infinity. In this case, with only two bursts observed from FRB 171019, it is not at all clear that this asymptotic form has been reached. Hence, we perform a toy simulation to test the validity of our assumption.

We use a simplified case, and consider only the R dimension, with other parameters fixed at $k = 0.34$, $\gamma = -0.9$, $\alpha = -1.5$. We assume a true rate $R = 1 \text{ day}^{-1}$, and simulate over the range $0.1 \leq R \leq 10 \text{ day}^{-1}$ for FRB 171019 using the same simulation of Section 3.7. Only the total number of bursts observed by each of the five receivers in Table 1 is recorded, i.e. no timing information is assumed. For each simulated observation, D is calculated by fitting cubic splines to the simulated probabilities of that result as a function of $\log R$. This allows the probability distribution $p(\text{obs}|R)$ to be smooth. Results where no repeat bursts were simulated were discarded. An example of the fitting procedure is shown in Fig. A1, while the resulting distribution of D is compared to a χ_1^2 distribution in Fig. ??.

From Fig. ??, it is evident that the broad form of D

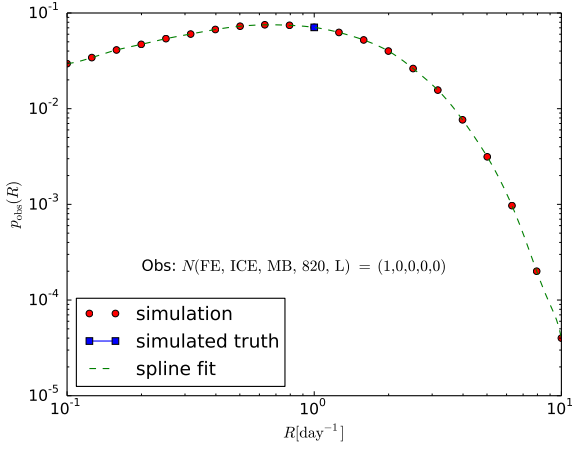


Figure A1. Red dots: simulated probability of observing one repeat burst from FRB 171019 with ASKAP Flye’s Eye mode ($N(\text{FE})=1$), and none with other instruments, as a function of repetition rate R , for $\gamma = -0.9$, $k = 0.34$, $\alpha = -1.5$. The simulated true value of R used to generate this observation is shown in blue. The green dashed line shows the spline fit.

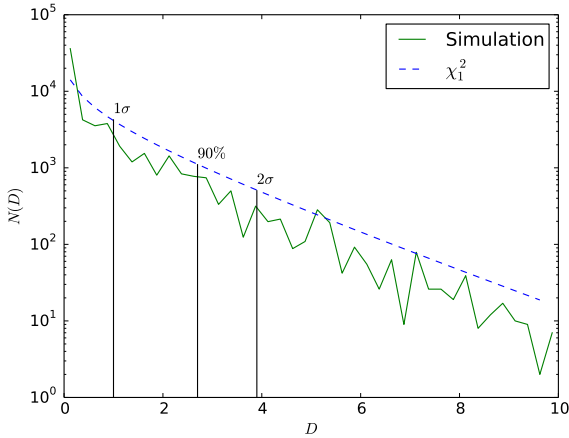


Figure A2. Simulated histogram of the test statistics D , compared to its expected χ_1^2 distribution, scaled to the number of simulations. Also shown (black lines) are characteristic cut-off values associated with 68% (1σ), 90%, and 95% (2σ) confidence levels.

is very similar to that of a χ_1^2 distribution. However, there is an excess near $D = 0$, and a deficit at larger values. A possible cause is the quantisation of FRB observations, i.e. only integer numbers of FRBs can be observed. Importantly, the true distribution of D lies at lower values than expected, meaning that confidence intervals set by assuming a χ_1^2 distribution will suffer from over-coverage, e.g. a 90% confidence limit may in fact be a 92% C.L. Extrapolating to the multi-dimensional cases treated in this work, we expect true parameter values to lie outside our 90% confidence regions less than 10% of the time.

This paper has been typeset from a $\text{\TeX}/\text{\LaTeX}$ file prepared by the author.